Parkin Dependent Mitophagy Protects Macrophage Against Oxidative Injury And Inflammation During Atherogenesis

Xiaopeng Liu (drxp_liu@126.com)
China-Japan Friendship Hospital https://orcid.org/0000-0002-7410-5767
Yanan Zhen
China-Japan Friendship Hospital
Xia Zheng
China-Japan Friendship Hospital
Yongxin Han
China-Japan Friendship Hospital
Qiangqiang Nie
China-Japan Friendship Hospital
Feng Wang
China-Japan Friendship Hospital
He Wang
Beijing Jiaotong University School of Science
Peng Liu
China-Japan Friendship Hospital

Research Article

Keywords: Mitophagy, Parkin, Mitochondria damage, Atherosclerosis, Macrophage, Oxidative stress

Posted Date: July 13th, 2021

DOI: https://doi.org/10.21203/rs.3.rs-684568/v1

Abstract

Mitochondrial oxidative injury induces macrophage inflammatory activation and apoptosis during atherogenesis. Timely clearance of dysfunctional mitochondria may therefore be beneficial for the survival of macrophages. Based on these principles, our working hypothesis was therefore that mitophagy mediated by the E3 ubiquitin ligase Parkin could have an important role in reducing both oxidative injury and the apoptosis of macrophages under atherogenic conditions. To examine this proposal, in the present study oxidative low-density lipoprotein (ox-LDL) treated THP-1 macrophages were used for the *in vitro* experiments, and high-cholesterol-fed male apolipoprotein E knockout ($ApoE^{-/-}$) mice were used for the *in vivo* investigations. The results demonstrated that mitophagy was activated both in oxidatively stimulated THP-1 macrophages and in aortic plaque macrophages of high-cholesterol-fed $ApoE^{-/-}$ mice. In ox-LDL treated THP-1 macrophages, both the expression level and mitochondrial translocation of Parkin were increased following oxidative stimulation, whereas silencing Parkin led to impaired mitophagy, which exacerbated macrophage oxidative injury, NF-κB activation and apoptosis. Taken together, these results have demonstrated that mitophagy exerts a protective role in macrophages under atherogenic conditions, and that Parkin is a key mediator in this process.

Introduction

Plaque destabilization and rupture is the primary cause of lethal complications of atherosclerotic cardiovascular disease (AS). The death of macrophages has been demonstrated to be strongly associated with plaque instability and rupture (1). Previous studies have shown that mitochondrial oxidative injury may accelerate macrophage death during atherogenesis (2–4). Damaged mitochondria may activate diverse cellular pathways, which ultimately leads to macrophage apoptosis (5–9). Furthermore, overproduction of reactive oxygen species (ROS) due to mitochondria dysfunction may activate the inflammation pathway, which also exacerbates atherosclerosis (6,10,11). The timely elimination of damaged mitochondria may therefore save macrophages from destruction, and alleviate AS.

Damaged mitochondria can be selectively degraded through the autophagy pathway, a process that is termed mitophagy (12). Mitophagy has been reported to play a salutary role in multiple cardiovascular diseases where oxidative stress and mitochondrial damage occur (13–15). In oxidative low-density lipoprotein (ox-LDL)-treated macrophage, mitophagy induced by melatonin was shown to attenuate IL-1β secretion (16). However, our understanding of mitophagy in the scope of AS is still far from comprehensive (15).

The E3 ubiquitin ligase Parkin has been recognized as an important mediator in mitophagy activation (17,18). Parkin normally resides in the cytosol; whereas, it is translocated to the outer mitochondria membrane (OMM) when mitochondrial depolarization arises (17,19). At the OMM, Parkin may ubiquitinate a subset of membrane proteins, facilitating their recognition and sequestration by the

autophagosome (20,21). In the present study, we investigated whether mitophagy could alleviate macrophage oxidative injury and inflammation, and also the role of Parkin in mitophagy initiation.

Our results demonstrated that both Parkin/mitochondria co-localization and mitochondria-autophagosome co-localization were identified in ox-LDL treated THP-1 macrophages, which implied that both Parkin mitochondrial translocation and mitophagy activation had occurred. Furthermore, the silencing of Parkin led to impaired mitophagy, which, in turn, accelerated macrophage inflammatory activation and apoptosis. Moreover, Parkin-mitochondria translocation and mitophagy activation were also demonstrated in aortic plaque macrophages of high-cholesterol-fed ApoE$^{-/-}$ mice.

Material And Methods

Cell culture and transfection. Human THP-1 monocytes obtained from the Cell Resource Center of Peking Union Medical College were cultured in Gibco® RPMI-1640 medium (cat. no. 61870-036; Thermo Fisher Scientific, Inc.) containing 10% Gibco fetal bovine serum (FBS) (cat. no. 10099-141; Thermo Fisher Scientific, Inc.). The THP-1 cells were differentiated into macrophages by adding 10 ng/ml phorbol 12-myristate 13-acetate (PMA) (cat. no. P8139; Merck KGaA) for 48 h. Subsequently, cells were washed twice with PBS and cultured for a further 48 h prior to treatment with ox-LDL.

Transfections and gene silencing were performed using Invitrogen Lipofectamine™ RNAiMAX (cat. no. 13778-075; Thermo Fisher Scientific, Inc.) according to the manufacturer's instructions. Parkin siRNA and control scrambled siRNA (cat. nos. sc-42158 and sc-37007, respectively; both from Santa Cruz Biotechnology, Inc.) at a concentration of 40 nM were transiently transfected into THP-1-derived macrophages and incubated for 24 h. Subsequently, cells were washed twice with PBS and cultured for a further 24 h. Then, cells were harvested and the post-nuclear supernatants were analyzed by western blotting to confirm knockdown of Parkin protein.

In vivo animal studies. In vivo protocols were approved by the hospital's Animal Studies Committee (No. 2017-6-36-GZR). Male apolipoprotein E knockout (ApoE$^{-/-}$) mice were obtained from the Institute of Laboratory Animal Science, Chinese Academy of Medical Science Peking University Medical College. For the atherosclerosis model, ApoE$^{-/-}$ mice were fed on a western diet containing 0.15% cholesterol, providing 42% calories as cholesterol (cat no. TD88137; Envigo), which began at 8 weeks of age.

After 8 weeks (early lesion) or 16 weeks (advanced lesion) of treatment, mice were sacrificed under general anesthesia with 2% isoflurane and blood was removed by perfusion with cold PBS. The aortas were rapidly dissected from the aortic root to the iliac bifurcation, peri-adventitial cholesterol and connective tissue were removed as much as possible, and the aortas were subsequently embedded and frozen in Tissue-Tek O.C.T. Compound (cat. no.4583; Sakura Finetek USA, Inc.), prior to being sealed and stored at -80°C.

Measurement of the mitochondria membrane potential (MMP) level. The MMP level was detected using the fluorescence indicator 5,5',6,6'-tetrachloro-1,1',3,3'-tetraethyl benzimidazolylcarbcyanine iodide (cat.

no. 70014; JC-1; Biotium, Inc.), in accordance with the manufacturer's instructions. In cells with a normal MMP, JC-1 forms aggregates that are detected as red fluorescence, whereas in cells with impaired MMP, the dye stays in a monomeric form that is detected as green fluorescence. The green-to-red fluorescence ratio was used as the measure of the MMP level as previously described (22).

Mitochondria mass analysis. Mitochondrial mass loss was measured by a FACS™ technique using Invitrogen MitoTracker™ Deep Red (cat. no. M22426; Thermo Fisher Scientific, Inc.) staining, as previously described (23). THP-1 macrophages were cultured with 50 nM MitoTracker Deep Red for 15 min at 37°C in the dark. After treatment, cells were trypsinized, washed and resuspended in Gibco Hank's balanced salt solution buffer. Subsequently, $1x10^5$ cells were acquired in the FL4 channels of an Accuri C6 flow cytometer (BD Biosciences).

Measurement of cellular ROS. Intracellular ROS were determined using 2',7'-dichlorofluorescein diacetate (DCF-DA) (cat. no. D6883; Merck KGaA) as previously described (23). The fluorescence intensity of each group was measured using an Accuri C6 flow cytometer (BD Biosciences), and quantified as the fold change compared with the baseline.

Measurement of mtROS. mtROS were determined using Molecular Probes® MitoSOX red (cat. no. M36008; Thermo Fisher Scientific, Inc.) as previously described (24). The fluorescence intensity of each group was measured by flow cytometry using an Accuri C6 flow cytometer (BD Biosciences), and quantified as the fold change compared with the baseline.

Dihydroethidium (DHE). Intracellular ROS were measured using dihydroethidium (DHE) (cat. no. D7008; Merck KGaA) in accordance with the manufacturer's protocol, as described previously (25). The fluorescence intensity of each group was measured by flow cytometry (BD Accuri C6) and quantified as the fold change compared with the baseline.

Immunofluorescence experiments. Cells cultured on coverslips were fixed with ice-cold methanol for 5 min, and then allowed to air-dry for 3 min. The coverslips were washed 3 times, 5 min per wash with PBS. Cells were subsequently blocked for 30 min with 5% goat serum. Primary antibodies used for the immunofluorescence experiments included rabbit-anti-parkin (cat. no.sc-32282; dilution, 1:50; Santa Cruz Biotechnology, Inc.), rabbit-anti-LC3A/B (cat. no. 4108; 1:200; Cell Signaling Technology, Inc.), rabbit-anti-Lamp1 (cat. no. ab24170; 1:200; Abcam), mouse-anti-COX IV (cat. no. 11967; 1:200; Cell Signaling Technology, Inc.) and rabbit-anti-p-NF-κB (Ser-536) (cat. no. 3033; 1:100; Cell Signaling Technology, Inc.). The primary antibodies were incubated for 1 h at 37°C. Following the incubation, cells were washed 3 times (5 min each wash) with PBS. Cells were subsequently incubated with either anti-rabbit AlexaFluor 488-conjugated (cat. no. A-11034) or anti-mouse AlexaFluor 594-conjugated (cat. no. A-11032; both from Thermo Fisher Scientific, Inc.) antibody for 30 min at room temperature in the dark. Coverslips were washed again as described above, and subsequently mounted using Fluoromount mounting media (cat. no. F4680; Merck KGaA).

Aortic sinus immunohistochemistry and histology. Cryostat sections (6 μm-thick) of the aortic sinus were cut parallel to the aortic root. Sections were subsequently stained with 200 nM MitoTracker Deep Red for 20 min at room temperature in the dark, washed with 1X PBS, and fixed for 5 min in ice-cold acetone. After fixation, sections were rinsed 3 times in PBS and blocked for 30 min in 5% goat serum. The aortic samples were subsequently incubated for 2 h at 37^{o}C with the primary antibodies rabbit-anti-Parkin (1:50), rabbit-anti-LC3B (cat. no. ab128025; 1:500; Abcam) and rat-anti-MOMA-2 (cat. no. ab33451; 1:50; Abcam), followed by washing and staining with the appropriate fluorescent secondary antibodies. Adjacent sections were stained with hematoxylin and eosin (Bio-Optica) and Oil Red (Merck KGaA) to determine the lesion area.

Confocal microscopy imaging and analysis. Coverslips and tissue sections were imaged using a laser scanning confocal microscope (TCS SP8 STED, 3x magnification; Leica Microsystems, Ltd.) equipped with a high-resolution AxioCam MRm digital camera (Carl Zeiss, Inc.). Images were deconvolved using Leica Application Suite Advanced Fluorescence software. Colocalization of Parkin or microtubule-associated protein 1 light chain 3 (LC3) protein (green fluorescence) with the mitochondria [mitochondrial cytochrome *c* oxidase subunit IV (COX IV) or MitoTracker Deep Red; red fluorescence] was analyzed and quantified using ImageJ software (National Institutes of Health), as previously described (26,27). At least 20 cells per sample were used for the *in vitro* studies, whereas n = 6 mice from each group were used for the *in vivo* study.

Preparation of cytosolic and mitochondrial proteins. Cytosolic and mitochondrial proteins of THP-1 macrophages were prepared using the cytosolic/mitochondria fractionation kits (C3601 kit for cells, and C3606 kit for tissues; Beyotime Institute of Biotechnology), in accordance with the manufacturer's instructions, as previously described (23).

Immunoblotting. Immunoblotting was performed as previously described (23). Aliquots of protein (15–20 μg/lane) were separated by 10 % sodium dodecyl sulfate-polyacrylamide gel electrophoresis (SDS-PAGE) and subjected to immunoblotting with the following antibodies: LC3A/B antibody (cat. no. 12741; 1:1,000), p62/SQSTM1 antibody (cat. no. 8025; 1:1,000), cytochrome *c* antibody (cat. no. 4272; 1:1,000), caspase-3 antibody (cat. no. 9662; 1:300), GAPDH antibody (cat. no. 2118; 1:1,000), COX IV antibody (1:1,000), p-NF-κB (Ser-536) antibody (cat. no. 8242; 1:1,000), and NF-κB antibody (cat. no. 4764; 1:1,000) (all from Cell Signal Technology); Parkin antibody (cat. no. sc-32282; 1:500) from Santa Cruz Biotechnology; Mfn2 antibody (cat. no. ab56889; 1:1000) and ubiquitin antibody (cat. no. ab134953; 1:200) from Abcam. The densities of the bands were measured using a Densitograph System (Ez-Capture II and CS Analyzer 3.0, ATTO, Tokyo, Japan), and the ratio to GAPDH was calculated.

Immunoprecipitation. THP-1 cells were harvested and resuspended in 1 ml of lysis buffer (150 mM NaCl, 50 mM Tris-HCl pH 7.6, 1% NP-40, 0.1% SDS, protease inhibitor cocktail (Roche Diagnostics)). Lysates were incubated on ice for 30 min and cleared by centrifugation at 13,000×g for 10 min. Samples were equalized for the protein concentration and incubated with 5 μl of anti-Mfn2 antibody overnight on a rotator. 50μl of washed protein G agarose beads (Roche Diagnostics) were added to the samples. This

was followed by incubation for 2 h on a rotator. Next, the beads were pelleted by centrifugation and the supernatant was discarded. The beads were washed three times with lysis buffer followed by resuspension into 2× loading buffer (Invitrogen) and incubation at 95°C for 5 min. After centrifugation, the supernatant was analyzed by Western blotting.

Detection of apoptosis by annexin-V/propidium iodide (AV/PI) dual staining. The THP-1 macrophages were incubated with ox-LDL for the indicated time periods, and subsequently processed with an annexin V-FITC Apoptosis Detection kit (cat. no. 556547; BD Biosciences), according to the manufacturer's instructions. Flow cytometric analysis was performed using an Accuri C6 flow cytometer (BD Biosciences). $5x10^3$ events per sample were collected into list mode files and analyzed using FlowJo software (version 7.6.1). The apoptotic rate was determined as the percentage of Q2 + Q4.

Electron microscopy. Electron microscopy was performed using a protocol previously described (28). Observations were made using a JEOL 1400 TEM microscope (JEOL, Ltd.) equipped with a side mount Gatan Orius SC1000 digital camera (Gatan, Inc.). Autophagic vacuoles (AVs) and mitochondria engulfed within AVs were identified as previously described (29).

Statistical analysis. All data are presented as the mean ± SEM (n = 3), unless otherwise stated in the Figure legends. Statistical analysis was performed using Student's t-test for two groups, and one-way analysis of variance for multiple groups. All analyses were performed using GraphPad Prism 6.0 (GraphPad Software, Inc.), and $P < 0.05$ was considered to indicate a statistically significant value.

Results

Ox-LDL-induced ROS overproduction and mitochondria damage in THP-1-derived macrophages. Ox-LDL has been recognized as a key athero-relevant inducer of oxidative stress (6). In the present study, we used ox-LDL-treated THP-1 macrophages, a verified model to study oxidative injury of mitochondria in macrophages (30,31). Both cellular and mitochondria ROS increased significantly as soon as 6 h following ox-LDL (60 µg/ml) treatment, and continued to increase up to 12 h (Fig. 1A and B). The effects of ox-LDL on mitochondrial membrane integrity were then assessed by monitoring the MMP using the JC-1 dye. After 12 h ox-LDL treatment, the THP-1 macrophages exhibited stronger green fluorescence and a higher green-to-red fluorescence ratio compared with untreated cells (Fig. 1C), suggesting a decrease in the MMP had occurred following ox-LDL treatment. Another feature of mitochondrial damage is loss of selective permeability of the mitochondria membrane, which, in turn, leads to the release of proapoptotic factors (2,7). Increased cytosol levels of cytochrome *c* and cleaved caspase-3 were identified in ox-LDL-treated macrophages (Fig. 1D). These results indicated that ox-LDL induces mitochondrial damage and ROS overproduction.

Ox-LDL-induced autophagy and mitophagy flux in macrophages. To assess autophagy and mitophagy activity in response to ox-LDL treatment, the expression levels of LC3-II and Beclin-1, both of which are recognized autophagosome markers, were first measured (32). The conversion of LC3-I into LC3-II is

indicative of autophagic activity, and the level of LC3-II present coincides well with the number of autophagosomes. Notably, it was found that ox-LDL treatment led to a marked increase in the levels of LC3-II and Beclin-1 (Fig. 2A). Functional autophagy denotes the dynamic process of autophagosome formation, cargo sequestration, and eventual lysosomal fusion/degradation, a process that is termed as ‘autophagic flux’ (33). The level of p62/SQSTM1, an ubiquitin- and LC3-binding adaptor protein that is inversely associated with autophagic flux, was subsequently examined (34). Incubation with ox-LDL led to the reduction of p62, indicating a functional autophagic flux (Fig. 2A).

In order to better differentiate autophagy induction from downstream inhibition, bafilomycin A1 was used to block the fusion of autophagosomes and lysosomes. The LC3-II level further increased following bafilomycin A1 treatment while p62 accumulated, which implied the presence of functional autophagic flux (Fig. S1).

Consistently, immunofluorescence staining revealed an increase in the numbers of LC3-positive puncta and their co-localization with the mitochondria marker, COX IV (Fig. 2B and C). Moreover, transmission electron microscopy (TEM) analysis provided direct evidence for mitophagy through observing autophagic structures containing mitochondrion-like cargoes, confirming the formation of mitophagosomes (Fig. 2D). In addition, sequestration of mitochondria into the lysosome compartments was confirmed by co-localization between COX IV and the lysosome marker LAMP-1 (Fig. 2E). Furthermore, mitochondria mass loss was determined by a recently described method with the help of MitoTracker Deep Red staining (Fig. 2F) (35). Together, these results indicated that functional mitophagy flux was induced in response to ox-LDL treatment.

Mitophagy activation in ox-LDL-treated macrophages is dependent on Parkin. The E3 ubiquitin ligase Parkin fulfills an important role in mitophagy activation (18). To explore the role of the Parkin in oxidative stress-induced mitophagy activation, both the level and the cellular location of Parkin were examined. As shown in Fig. 3A, the total level of cellular Parkin showed a slight, but notable, increase at 12 h following ox-LDL treatment. Furthermore, the level of Parkin in the mitochondrial fraction was significantly increased, suggesting the translocation of Parkin to the mitochondria (Fig. 3A), which was further evidenced by immunofluorescence staining (Fig. 3B). As previously reported, PINK1 played an import role in recruitment and activation of Parkin after identifying and anchoring on damaged mitochondria (14,15). Accordingly, we found increased PINK1 level in the mitochondrial fraction after ox-LDL treatment in THP-1 macrophages (Fig. 3A). Once activated, Parkin can lead to ubiquitination of a series of mitochondrial membrane proteins, such as Mfn2 (20,21). To test the function of Parkin, we performed immunoprecipitation using an antibody against Mfn2. The resulting immunoprecipitates were analyzed by Western blotting with antibodies against ubiquitin and against Mfn2. Increased ubiquitination level of Mfn2 was demonstrated after ox-LDL incubation, which implied the activation of Parkin (Fig. 3A). It has been reported that polyubiquitination catalyzed by Parkin gives rise to the recruitment of p62 to damaged mitochondria, facilitating their recognition by autophagosomes (20). The levels of p62 and LC3 I/II were then measured in the mitochondria fraction. The results revealed that the levels of p62 and LC3 increased concomitantly with that of Parkin in the mitochondrial fraction following ox-LDL stimulation (Fig. 3A).

Furthermore, to facilitate our analysis of the importance of Parkin in mitophagy, Parkin was silenced, which led to decreased p62 and LC3 levels in the mitochondrial compartment (Fig. 3C). Immunofluorescence staining revealed that knocking down Parkin protein led to a decrease in the extent of mitochondrion-autophagosome co-localization in the macrophages (Fig. 3D and E). Moreover, TEM images revealed a high density of non-functional autophagosomes in Parkin-silenced macrophages, as well as the intracellular accumulation of mitochondrial fragments (Fig. 3F). Taken together, these results suggested that Parkin is essential for mitophagy activation in response to ox-LDL simulation.

Mitophagy impairment by silencing Parkin aggravates macrophage oxidative injury and apoptosis. To further understand the role of mitophagy in ox-LDL-induced oxidative stress, mitophagy was impaired via silencing Parkin. The results revealed that impaired mitophagy resulted in an elevated cellular green-to-red JC-1 ratio and an increase in the mitoSOX intensity of THP-1 macrophages both with and without ox-LDL treatment (Fig. 4A and B). Moreover, silencing Parkin further exacerbated the release of cytochrome *c* and caspase-3 activation in ox-LDL-treated THP-1 macrophages (Fig. 4C). Since both mitochondrial damage and ROS accumulation are known to be strong inducers of apoptosis, macrophage apoptosis was quantified by performing AV/PI dual staining. As shown in Fig. 4D and E, 12 h of ox-LDL treatment led to a marked increase in the ratio of AV-positive macrophages, which was increased even further when Parkin was knocked down. Furthermore, mtROS have recently been associated with inflammation via the NF-κB pathway (6). Subsequently, the effect of mitophagy on NF-κB pathway activation in atherogenic macrophages was investigated next. Figure 4F and G show the phosphorylation (Ser-536) and nuclear translocation of RelA (NF-κB p65) after ox-LDL treatment. Silencing of Parkin led to a further increase in NF-κB p65 activation, possibly due to defective mitophagy and mtROS elimination.

Activation of mitophagy in the plaque macrophages of ApoE $^{-/-}$ mice. In order to further validate our findings *in vivo*, whether or not mitophagy was also activated in plaque macrophages of high-cholesterol fed ApoE$^{-/-}$ mice was subsequently explored. Aortic root sections of ApoE$^{-/-}$ mice were immunostained with the MOMA-2 antibody to identify macrophages in lesions (Fig. 5A). Both in early (8 weeks) and advanced (16 weeks) lesions, immunofluorescence staining provided clear evidence of autophagosome and mitophagosome formation (Fig. 5B). Mitophagy activation was further confirmed by observation of autophagic structures containing mitochondrion-like cargoes under the TEM microscope (Fig. 5C). Subsequently, whether or not Parkin also participates in mitophagy activation was investigated. As shown in Fig. 5D, mitochondrial translocation of Parkin was also promoted in plaque macrophages of high-cholesterol-fed ApoE$^{-/-}$ mice. Moreover, the levels of both Parkin and p62 in the mitochondrial fraction of the aorta lysis were significantly increased upon atherosclerosis development (Fig. 5E).

Discussion

Macrophages occupy a central role during the pathogenesis of atherosclerosis (1). Increasing lines of evidence suggest that mitochondrial oxidative injury, and the subsequent overproduction of mtROS, is closely associated with macrophage death and plaque destabilization (2). Physiologically, mtROS is a natural by-product of the respiratory chain, and performs important signaling functions as an intracellular

messenger (36,37). During atherogenesis, progressive mitochondrial damage and respiratory chain dysfunction develops in macrophages in lesions due to severe and prolonged oxidative stress (4,38–40). Damaged mitochondria thereby become a major source of cellular ROS, which continuously amplify the oxidative injuries via impairing adjacent mitochondria and exacerbating mtROS production in a feed-forward manner (41). In the present study, rapid mitochondria injury and mtROS accumulation were observed in ox-LDL-treated THP-1 macrophages. Furthermore, increased lesional ROS levels were revealed as atherosclerosis progressed in ApoE$^{-/-}$ mice. It is therefore of paramount importance that dysfunctional mitochondria should be eliminated in a timely manner to prevent further damage.

Autophagy is the natural destructive mechanism that orderly degrades and recycles unnecessary or dysfunctional cellular components. In recent years, autophagy and mitophagy have been widely reported in multiple cardiovascular diseases including AS (14,15). Macrophages and foam cells are the predominant component consist the lipid core of atherosclerotic plaque. Macrophage autophagy has already been demonstrated to have an anti-atherogenic effect (42,43). However, the underlying mechanism(s) has yet to be properly elucidated. Previous studies have proposed that potential mechanisms may involve the autophagic removal of damaged mitochondria, in turn reducing ROS injuries (43,44). In the present study, direct evidence has been provided to demonstrate mitophagy activation in oxidative-stimulated macrophages. Damaged mitochondria were shown to be sequestrated and degraded through the autophagosome-lysosome pathway, and the importance of this process was highlighted by an accelerated rate of inflammatory activation and cell apoptosis in macrophages with impaired mitophagy. Vascular smooth muscle cells (VSMCs) are another important cellular component of atherosclerotic plaque and the main component of the fibrous cap. Autophagy and mitophagy have also been reported in VSMCs. Defect mitophagy in VSMCs is closely related to cell apoptosis and unstable atherosclerotic plaque phenotype (45,46). Therefore, autophagy and mitophagy play an important role in plaque stabilization and may become a potential target for anti-atherogenic therapy.

The E3 ubiquitin ligase Parkin has been recognized as an important mediator in mitophagy activation in a variety of neuromuscular and cardiovascular diseases (47–49). However, the role of Parkin in atherosclerosis development has yet to be properly examined. In the present study, it has been demonstrated that Parkin is upregulated and translocated to the mitochondria under oxidative conditions, and that the protein is essential for macrophage mitophagy activation both *in vitro* and *in vivo*. Knocking down Parkin leads to impaired mitophagy with intracellular retention of mtROS, which promotes macrophage inflammatory activation and cell apoptosis. Possible roles of Parkin and mitophagy during atherogenesis are summarized in Fig. 6. It is worth noting that Parkin-mediated mitochondrial ubiquitination may have different roles in mitochondrial degradation. Upon mitochondrial membrane depolarization, proteasomes are recruited to the mitochondria in a Parkin-dependent manner, leading to the degradation of proteins located at the OMM and intermembrane space, but not in the inner membrane or the matrix (50). Therefore, immunostaining for mitochondrial inner membrane or matrix proteins, such as CypD and COX IV, would be more appropriate for monitoring mitophagy (51).

Interestingly, ROS have been shown to participate in almost all aspects of macrophage-associated atherogenic processes, including oxidative modification of LDL, monocyte recruitment, macrophage activation, efferocytosis and extracellular matrix degradation (52–54). Therefore, in addition to suppressing macrophage inflammatory activation and apoptosis, the anti-atherogenic effect of mitophagy may be involved in all the pathological processes in which ROS participates. Moreover, a link between ROS and autophagy activation has recently been revealed, and recognized as a self-protective mechanism of cells (55–57). Known mechanisms for ROS-induced autophagy include direct suppression of mammalian target of rapamycin (mTOR) activity and transcriptional regulation of autophagy-associated genes (55,58,59). Therefore, in addition to leading to mitochondrial injury and an accumulation of Parkin, mtROS may be able to directly induce mitophagy through upregulating autophagosome formation. However, those hypotheses need to be confirmed in subsequent studies.

Conclusion

The present study has demonstrated that an accumulation of damaged mitochondria leads to macrophage oxidative injury and atherogenesis. It has been shown that mitophagy serves an important role in eliminating mitochondria and in decelerating the development of atherosclerosis. Mitophagy may therefore provide a promising target for therapeutic intervention in the treatment of atherosclerosis.

Declarations

Author Contribution Statement

Xiaopeng Liu: Conceptualization (lead); data Curation (lead); writing-original draft (lead); formal analysis (equal); funding Acquisition (lead). Yanan Zhen: Software (lead); methodology (lead). Xia Zheng: Investigation (lead); methodology (equal); formal Analysis (equal). Yongxin Han: Project Administration (lead); investigation (equal); methodology (equal); software (equal). Qiangqiang Nie: Formal Analysis (lead); investigation (equal). Feng Wang: Investigation (equal); methodology (equal); resources (equal). He Wang: Resources (lead); software (equal); data Curation (equal). Peng Liu: Supervision (lead); visualization (lead); writing-review & editing (lead); conceptualization (equal); funding Acquisition (equal).

Funding

This work was supported by the Natural Science Foundation of China (grant no. 81700399).

Conflicts of interest

The authors declare they have no competing interests.

Availability of data and material

The data that support the findings of this study are available from the corresponding author upon reasonable request.

Code availability

All data, models, or code generated or used during the study are available from the corresponding author by request.

Ethics approval

In vivo protocols were approved by the hospital's Animal Studies Committee (No. 2018-6-36-GZR)

References

1. Moore KJ, Tabas I. Macrophages in the pathogenesis of atherosclerosis. Cell 2011; 145:341 – 55.

2. Madamanchi NR, Runge MS. mitochondria dysfunction in atherosclerosis. Circ Res 2007; 100:460 – 73.

3. Marchant CE, Law NS, van der Veen C, Hardwick SJ, Carpenter KL, Mitchinson MJ. Oxidized low-density lipoprotein is cytotoxic to human monocyte-macrophages: protection with lipophilic antioxidants. FEBS Lett 1995; 358:175-8.

4. Wintergerst ES, Jelk J, Rahner C, Asmis R. Apoptosis induced by oxidized low density lipoprotein in human monocyte-derived macrophages involves CD36 and activation of caspase-3. Eur J Biochem 2000; 267:6050-9.

5. Wang Y, Tabas I. Emerging roles of mitochondria ROS in atherosclerotic lesions: causation or association. J Atheroscler Thromb 2014; 21:381 – 90.

6. Wang Y, Wang GZ, Rabinovitch PS, Tabas I. Macrophage mitochondria oxidative stress promotes atherosclerosis and nuclear factor-kappaB-mediated inflammation in macrophages. Circ Res 2014; 114:421 – 33.

7. Sinha K, Das J, Pal PB, Sil PC. Oxidative stress: the mitochondria-dependent and mitochondria-independent pathways of apoptosis. Arch Toxicol 2013; 87:1157-80.

8. Suen DF, Norris KL, Youle RJ. mitochondria dynamics and apoptosis. Genes Dev 2008; 22:1577-90.

9. Asmis R, Begley JG. Oxidized LDL promotes peroxide-mediated mitochondria dysfunction and cell death in human macrophages: a caspase-3-independent pathway. Circ Res 2003; 92:e20-9.

10. Zhou R, Yazdi AS, Menu P, Tschopp J. A role for mitochondria in NLRP3 inflammasome activation. Nature 2011; 469:221-5.

11. Ding Z, Liu S, Wang X, Khaidakov M, Dai Y, Mehta JL. Oxidant stress in mitochondria DNA damage, autophagy and inflammation in atherosclerosis. Sci Rep 2013; 3:1077.

12. Youle RJ, Narendra DP. Mechanisms of mitophagy. Nat Rev Mol Cell Biol 2011; 12:9–14.

13. Bravo-San Pedro JM, Kroemer G, Galluzzi L. Autophagy and Mitophagy in Cardiovascular Disease. Circ Res. 2017;120(11):1812–1824.

14. Morciano G, Patergnani S, Bonora M, et al. Mitophagy in Cardiovascular Diseases. J Clin Med. 2020;9(3):892.

15. Poznyak AV, Nikiforov NG, Wu WK, Kirichenko TV, Orekhov AN. Autophagy and Mitophagy as Essential Components of Atherosclerosis. Cells. 2021;10(2):443.

16. Ma S, Chen J, Feng J, et al. Melatonin Ameliorates the Progression of Atherosclerosis via Mitophagy Activation and NLRP3 Inflammasome Inhibition. Oxid Med Cell Longev. 2018;2018:9286458.

17. Narendra D, Tanaka A, Suen DF, Youle RJ. Parkin is recruited selectively to impaired mitochondria and promotes their autophagy. J Cell Biol 2008; 183:795–803.

18. Narendra DP, Jin SM, Tanaka A, Suen DF, Gautier CA, Shen J, et al. PINK1 is selectively stabilized on impaired mitochondria to activate Parkin. PLoS Biol 2010; 8:e1000298.

19. Wang Y, Nartiss Y, Steipe B, McQuibban GA, Kim PK. ROS-induced mitochondria depolarization initiates PARK2/PARKIN-dependent mitochondria degradation by autophagy. Autophagy 2012; 8:1462-76.

20. Geisler S, Holmstrom KM, Skujat D, Fiesel FC, Rothfuss OC, Kahle PJ, et al. PINK1/Parkin-mediated mitophagy is dependent on VDAC1 and p62/SQSTM1. Nat Cell Biol 2010; 12:119 − 31.

21. Vives-Bauza C, Zhou C, Huang Y, Cui M, de Vries RL, Kim J, et al. PINK1-dependent recruitment of Parkin to mitochondria in mitophagy. Proc Natl Acad Sci U S A 2010; 107:378 − 83.

22. Keil VC, Funke F, Zeug A, Schild D, Muller M. Ratiometric high-resolution imaging of JC-1 fluorescence reveals the subcellular heterogeneity of astrocytic mitochondria. Pflugers Arch 2011; 462:693–708.

23. Li K, Cui YC, Zhang H, Liu XP, Zhang D, Wu AL, et al. Glutamine Reduces the Apoptosis of H9C2 Cells Treated with High-Glucose and Reperfusion through an Oxidation-Related Mechanism. PLoS One 2015; 10:e0132402.

24. Piacenza L, Irigoin F, Alvarez MN, Peluffo G, Taylor MC, Kelly JM, et al. mitochondria superoxide radicals mediate programmed cell death in Trypanosoma cruzi: cytoprotective action of mitochondria iron superoxide dismutase overexpression. Biochem J 2007; 403:323 − 34.

25. Lee IO, Kratz MT, Schirmer SH, Baumhakel M, Bohm M. The effects of direct thrombin inhibition with dabigatran on plaque formation and endothelial function in apolipoprotein E-deficient mice. J Pharmacol Exp Ther 2012; 343:253-7.

26. Andres AM, Hernandez G, Lee P, Huang C, Ratliff EP, Sin J, et al. Mitophagy is required for acute cardioprotection by simvastatin. Antioxid Redox Signal 2014; 21:1960-73.

27. Ding WX, Ni HM, Li M, Liao Y, Chen X, Stolz DB, et al. Nix is critical to two distinct phases of mitophagy, reactive oxygen species-mediated autophagy induction and Parkin-ubiquitin-p62-mediated mitochondria priming. J Biol Chem 2010; 285:27879-90.

28. Singh R, Kaushik S, Wang Y, Xiang Y, Novak I, Komatsu M, et al. Autophagy regulates lipid metabolism. Nature 2009; 458:1131-5.

29. Chu CT. A pivotal role for PINK1 and autophagy in mitochondria quality control: implications for Parkinson disease. Hum Mol Genet 2010; 19:R28-37.

30. Zhu M, Du J, Liu AD, Holmberg L, Chen SY, Bu D, et al. L-cystathionine inhibits oxidized low density lipoprotein-induced THP-1-derived macrophage inflammatory cytokine monocyte chemoattractant protein-1 generation via the NF-kappaB pathway. Sci Rep 2015; 5:10453.

31. Li G, Peng J, Liu Y, Li X, Yang Q, Li Y, et al. Oxidized low-density lipoprotein inhibits THP-1-derived macrophage autophagy via TET2 down-regulation. Lipids 2015; 50:177 – 83.

32. Klionsky DJ, Abdalla FC, Abeliovich H, Abraham RT, Acevedo-Arozena A, Adeli K, et al. Guidelines for the use and interpretation of assays for monitoring autophagy. Autophagy 2012; 8:445–544.

33. Mizushima N, Yoshimori T, Levine B. Methods in mammalian autophagy research. Cell 2010; 140:313 – 26.

34. Mathew R, Karp CM, Beaudoin B, Vuong N, Chen G, Chen HY, et al. Autophagy suppresses tumorigenesis through elimination of p62. Cell 2009; 137:1062-75.

35. Mauro-Lizcano M, Esteban-Martinez L, Seco E, Serrano-Puebla A, Garcia-Ledo L, Figueiredo-Pereira C, et al. New method to assess mitophagy flux by flow cytometry. Autophagy 2015; 11:833 – 43.

36. Turrens JF. mitochondria formation of reactive oxygen species. J Physiol 2003; 552:335 – 44.

37. Finkel T. Signal transduction by mitochondria oxidants. J Biol Chem 2012; 287:4434-40.

38. Yao PM, Tabas I. Free cholesterol loading of macrophages is associated with widespread mitochondria dysfunction and activation of the mitochondria apoptosis pathway. J Biol Chem 2001; 276:42468-76.

39. Ling WH, Wang LL, Ma J. Supplementation of the black rice outer layer fraction to rabbits decreases atherosclerotic plaque formation and increases antioxidant status. J Nutr 2002; 132:20 – 6.

40. Tuominen A, Miller YI, Hansen LF, Kesaniemi YA, Witztum JL, Horkko S. A natural antibody to oxidized cardiolipin binds to oxidized low-density lipoprotein, apoptotic cells, and atherosclerotic lesions. Arterioscler Thromb Vasc Biol 2006; 26:2096 – 102.

41. Saito T, Sadoshima J. Molecular mechanisms of mitochondria autophagy/mitophagy in the heart. Circ Res 2015; 116:1477-90.

42. Maiuri MC, Grassia G, Platt AM, Carnuccio R, Ialenti A, Maffia P. Macrophage autophagy in atherosclerosis. Mediators Inflamm 2013; 2013:584715.

43. Razani B, Feng C, Coleman T, Emanuel R, Wen H, Hwang S, et al. Autophagy links inflammasomes to atherosclerotic progression. Cell Metab 2012; 15:534 – 44.

44. Liao X, Sluimer JC, Wang Y, Subramanian M, Brown K, Pattison JS, et al. Macrophage autophagy plays a protective role in advanced atherosclerosis. Cell Metab 2012; 15:545 – 53.

45. Osonoi Y, Mita T, Azuma K, et al. Defective autophagy in vascular smooth muscle cells enhances cell death and atherosclerosis. Autophagy. 2018;14(11):1991–2006.

46. Nahapetyan H, Moulis M, Grousset E, et al. Altered mitochondrial quality control in Atg7-deficient VSMCs promotes enhanced apoptosis and is linked to unstable atherosclerotic plaque phenotype. Cell Death Dis. 2019;10(2):119.

47. Dodson MW, Guo M. Pink1, Parkin, DJ-1 and mitochondria dysfunction in Parkinson's disease. Curr Opin Neurobiol 2007; 17:331-7.

48. Huang C, Andres AM, Ratliff EP, Hernandez G, Lee P, Gottlieb RA. Preconditioning involves selective mitophagy mediated by Parkin and p62/SQSTM1. PLoS One 2011; 6:e20975.

49. Kubli DA, Zhang X, Lee Y, Hanna RA, Quinsay MN, Nguyen CK, et al. Parkin protein deficiency exacerbates cardiac injury and reduces survival following myocardial infarction. J Biol Chem 2013; 288:915 – 26.

50. Yoshii SR, Kishi C, Ishihara N, Mizushima N. Parkin mediates proteasome-dependent protein degradation and rupture of the outer mitochondria membrane. J Biol Chem 2011; 286:19630-40.

51. Ding WX, Yin XM. Mitophagy: mechanisms, pathophysiological roles, and analysis. Biol Chem 2012; 393:547 – 64.

52. Violi F, Basili S, Nigro C, Pignatelli P. Role of NADPH oxidase in atherosclerosis. Future Cardiol 2009; 5:83–92.

53. McPhillips K, Janssen WJ, Ghosh M, Byrne A, Gardai S, Remigio L, et al. TNF-alpha inhibits macrophage clearance of apoptotic cells via cytosolic phospholipase A2 and oxidant-dependent mechanisms. J Immunol 2007; 178:8117-26.

54. Rajagopalan S, Meng XP, Ramasamy S, Harrison DG, Galis ZS. Reactive oxygen species produced by macrophage-derived foam cells regulate the activity of vascular matrix metalloproteinases in vitro.

Implications for atherosclerotic plaque stability. J Clin Invest 1996; 98:2572-9.

55. Lee J, Giordano S, Zhang J. Autophagy, mitochondria and oxidative stress: cross-talk and redox signalling. Biochem J 2012; 441:523 – 40.

56. Scherz-Shouval R, Elazar Z. Regulation of autophagy by ROS: physiology and pathology. Trends Biochem Sci 2011; 36:30 – 8.

57. Azad MB, Chen Y, Gibson SB. Regulation of autophagy by reactive oxygen species (ROS): implications for cancer progression and treatment. Antioxid Redox Signal 2009; 11:777 – 90.

58. Scherz-Shouval R, Shvets E, Fass E, Shorer H, Gil L, Elazar Z. Reactive oxygen species are essential for autophagy and specifically regulate the activity of Atg4. EMBO J 2007; 26:1749-60.

59. Groenewoud MJ, Zwartkruis FJ. Rheb and mammalian target of rapamycin in mitochondria homoeostasis. Open Biol 2013; 3:130185.

Figures

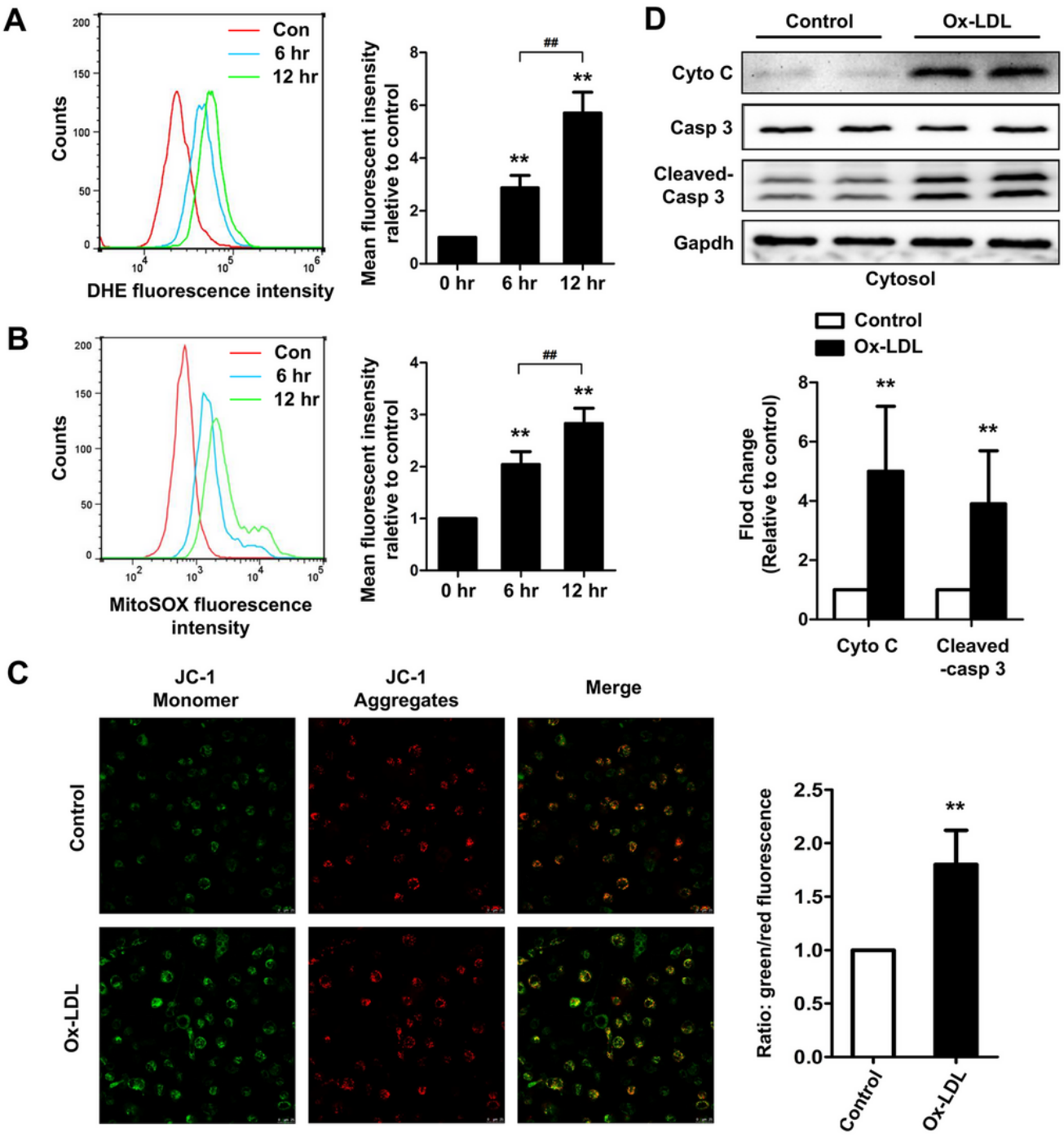

Figure 1

Ox-LDL induced ROS overproduction and mitochondria damage in THP-1 derived macrophage. THP-1 macrophages were treated with ox-LDL (60 μg/ml) for the indicated time periods. Representative cytofluorimetric analysis (left panel) and a graph showing quantitative analysis (right panel) of (A) cellular and (B) mitochondrial ROS. **P<0.01 vs. untreated (0 h) group; ##P<0.01 between indicated groups. (C) THP-1 macrophages were treated with vehicle control or ox-LDL (60 μg/ml) for 12 h.

Representative images of JC-1 confocal images of each group (left panel), and quantitative analysis (right panel) of the JC-1 fluorescence using a microplate reader (n=4), are shown. **P<0.01 vs. control group. Scale bar, 25 μm. (D) Cells were treated as described in (C), and representative immunoblots and densitometric graphs of cytosolic cytochrome c and cleaved caspase-3 levels normalized against GAPDH are shown. **P<0.01 vs. control group. Ox-LDL, oxidative low-density lipoprotein; ROS, reactive oxygen species.

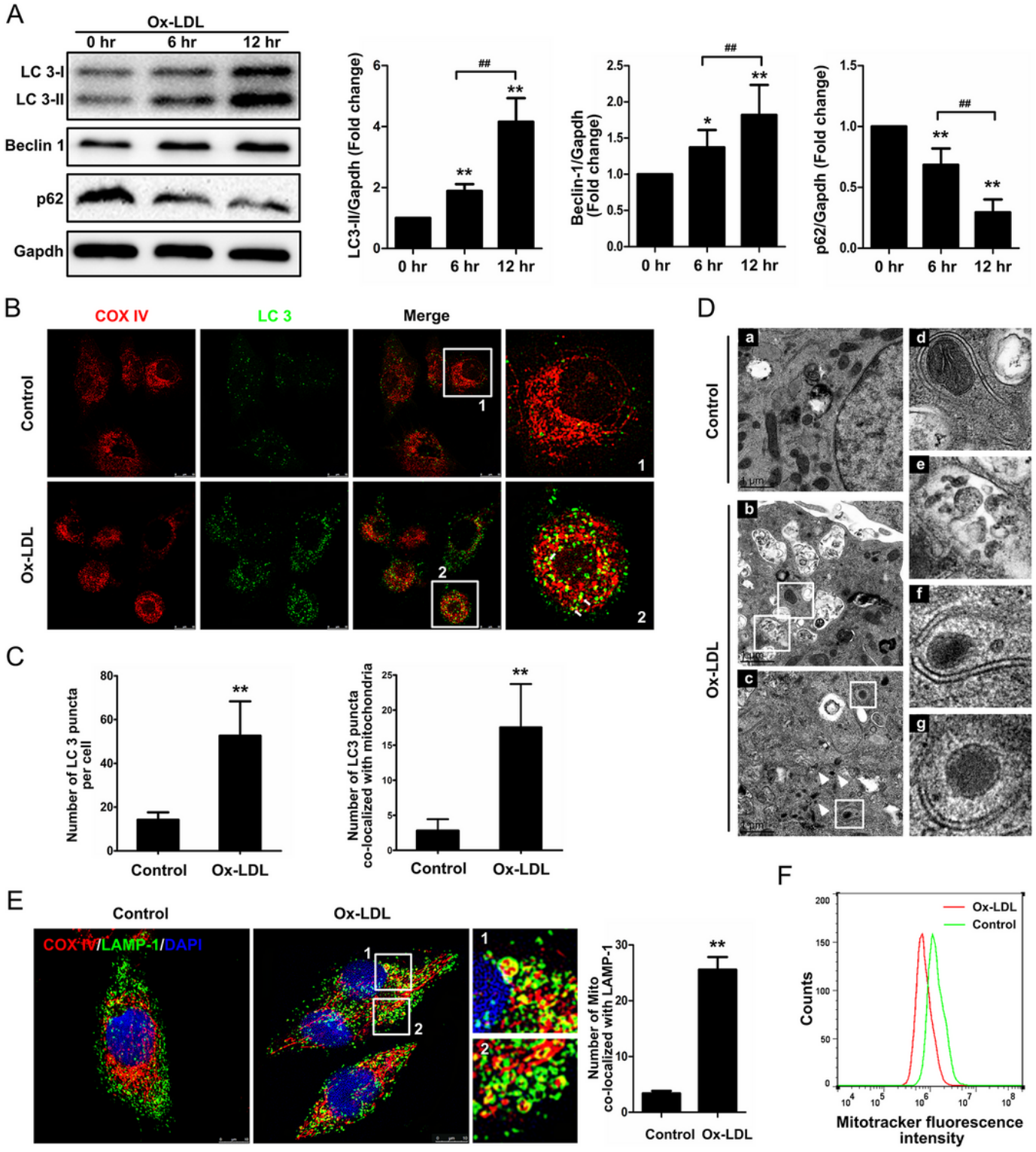

Figure 2

Ox-LDL-induced autophagy and mitophagy flux in macrophages. THP-1 macrophages were treated with vehicle control or ox-LDL (60 μg/ml) for 12 h. (A) Representative immunoblots and densitometric graphs of cellular LC3-II, Beclin-1 and p62 levels normalized against GAPDH. *P<0.05 vs. control group, **P<0.01 vs. control group; ##P<0.01 between indicated groups. (B) Cells were immunostained with the autophagy marker, LC3 (green) and mitochondria marker COX IV (red). Boxes indicate regions enlarged on the right, whereas the arrows (yellow puncta) indicate LC3 puncta (green) colocalized with mitochondria (red). Scale bar, 10 μm. (C) Quantification of the numbers of total LC3 puncta and LC3 puncta colocalized with mitochondria (n=5). **P<0.01 vs. control group. (D) Representative transmission electron micrographs showing normal mitochondria in (a) the control group, and (b) autophagic structures containing mitochondrion-like cargoes in the ox-LDL-treated group. The right panels were enlarged from the boxed area in the left panels, showing (d), (f) and (g) early autophagosomes, and (e) autolysosomes. Arrowheads indicate the mitochondria fragments. (E) Cells were immunostained with antibodies against LAMP-1 (green) and COX IV (red). Representative images (left panel; boxes indicate regions enlarged on the right), and quantification of the number of mitochondria colocalized with LAMP-1 per cell (right panel), are shown. **P<0.01 vs. control group. Scale bar, 10 μm. (F) Cells were incubated with MitoTracker Deep Red, and detected using the flow cytometry. Ox-LDL, oxidative low-density lipoprotein; COX IV, cytochrome c oxidase subunit IV; LC3, microtubule-associated protein 1 light chain 3.

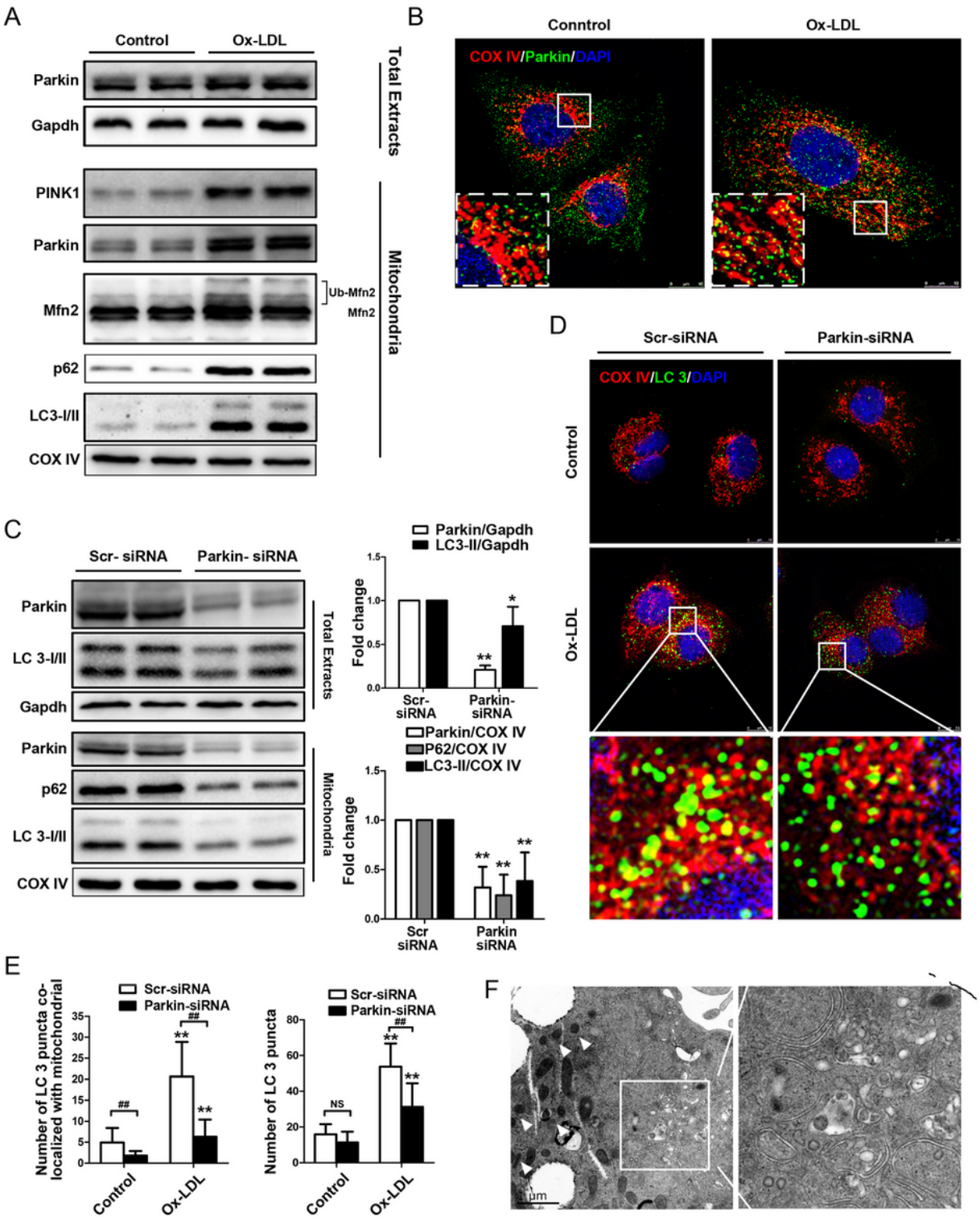

Figure 3

Mitophagy activation in ox-LDL-treated macrophages is dependent on Parkin. (A) THP-1 macrophages were treated with vehicle control or ox-LDL (60 μg/ml) for 12 h. Representative immunoblots and densitometric graphs of total cellular content of Parkin (normalized against GAPDH) and the mitochondrial content of PINK1, Parkin, Mfn2/Ub-Mfn2, p62 and LC3-II (normalized against COX IV) are shown. *P<0.05 vs. control, **P<0.01 vs. control. (B) THP-1 macrophages were treated as described in (A).

Cells were immunostained with antibodies against Parkin (green) and COX IV (red). Boxes indicate regions enlarged at the lower-left corner. Scale bar, 10 μm. (C) THP-1 macrophages were transfected with scrambled (scr) or Parkin siRNA, followed by ox-LDL treatment (60 μg/ml) for 12 h. Representative immunoblots and densitometric graphs of total cellular content of Parkin and LC3-II (against GAPDH) and mitochondrial content of Parkin, p62 and LC3-II (normalized against COX IV) are shown. **P<0.01 vs. ScrsiRNA group. (D) THP-1 macrophages were transfected with scrambled or Parkin siRNA, followed by treatment with vehicle control or ox-LDL (60 μg/ml) for 12 h. Cells were immunostained with LC3 (green) and COX IV (red). Scale bar, 10 μm.(E) Quantification of the number of total LC3 puncta and LC3 puncta colocalized with mitochondria. **P<0.01 vs. control group; ##P<0.01 between indicated groups; NS, not significant (P>0.05). (F) THP-1 macrophages were transfected with Parkin siRNA followed by ox-LDL treatment (60 μg/ml) for 12 h. Representative transmission electron micrographs are shown, demonstrating non-functional autophagosomes (box) and accumulated mitochondria fragments (arrowheads). Ox-LDL, oxidative low-density lipoprotein; Ub-Mfn2, ubiquitinated Mfn2; COX IV, cytochrome c oxidase subunit IV; LC3, microtubule-associated protein 1 light chain 3.

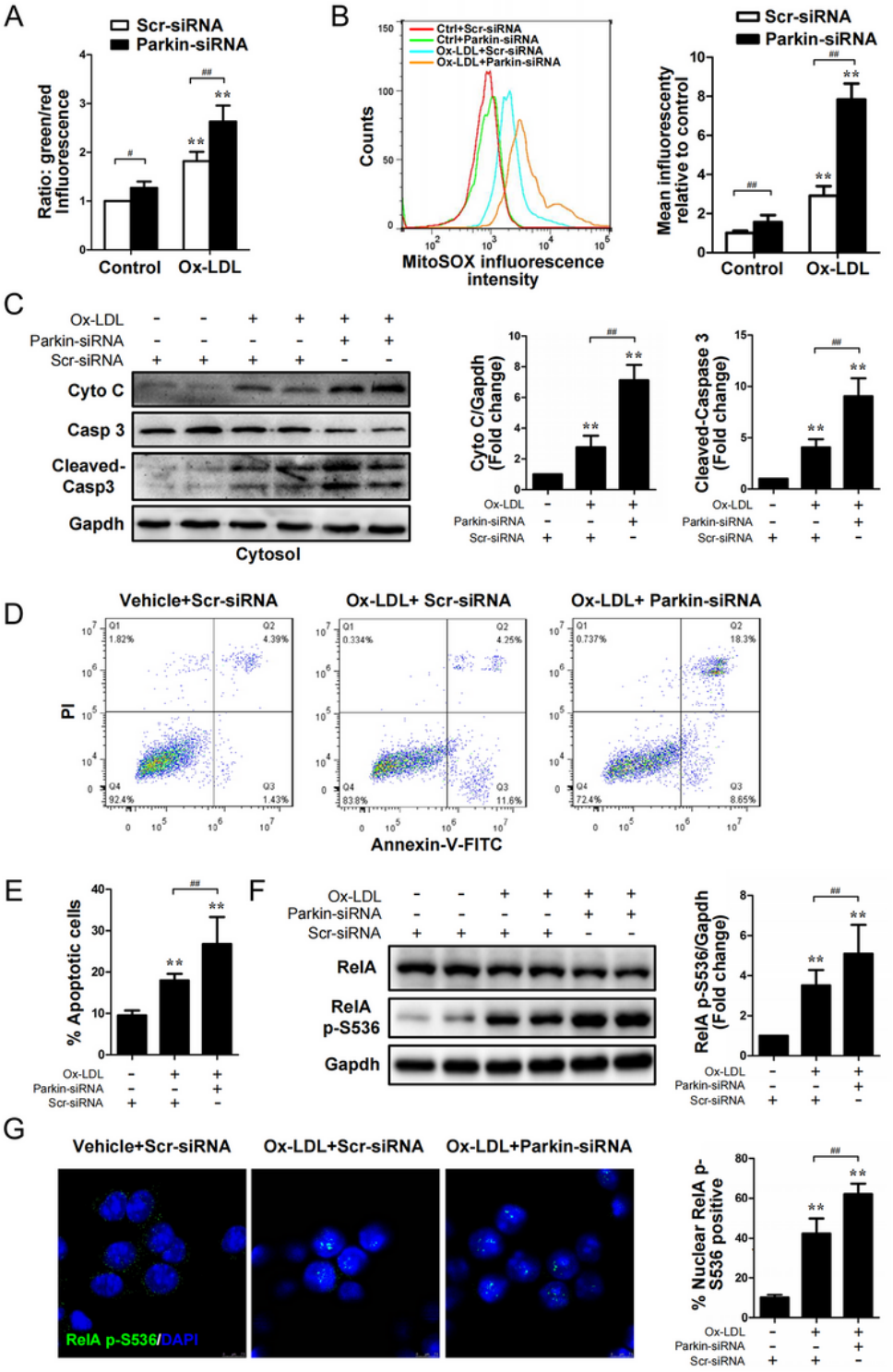

Figure 4

Mitophagy defects induced by silencing Parkin promote atherosclerosis. THP-1 macrophages were transfected with scrambled (scr) or Parkin siRNA, followed by treatment with vehicle control or ox-LDL (60 μg/ml) for 12 h. (A) Quantitative analysis of JC-1 fluorescence using a microplate reader (n=4). **P<0.01 vs. control; #P<0.05, ##P<0.01 between indicated groups. (B) Representative cytofluorimetric analysis (left panel) and graph showing quantitative analysis (right panel) of mtROS. **P<0.01 vs. control;

##P<0.01 between indicated groups. (C) Representative immunoblots and densitometric graph of cytosolic cytochrome c and cleaved caspase-3 levels normalized against GAPDH. (D) Cells were stained with annexin V-FITC and propidium iodide, and analyzed by flow cytometry. (E) Quantitative data of the apoptotic cells (n=4). (F) Representative immunoblots and densitometric graphs of cellular RelA and RelA-phosphorylated (p)-Ser-536 levels normalized against GAPDH. (G) Cells were immunostained with antibody against RelA pS536 (green). Representative immunofluorescence images (left panel) and quantification of p-Ser-536-positive RelA in the nuclei per cell (right panel) are shown. Scale bar, 7.5 μm. For (C-G), **P<0.01 vs. vehicle + Scr-siRNA; ##P<0.01 between indicated groups. Ox-LDL, oxidative low-density lipoprotein; mtROS, mitochondria-derived reactive oxygen species.

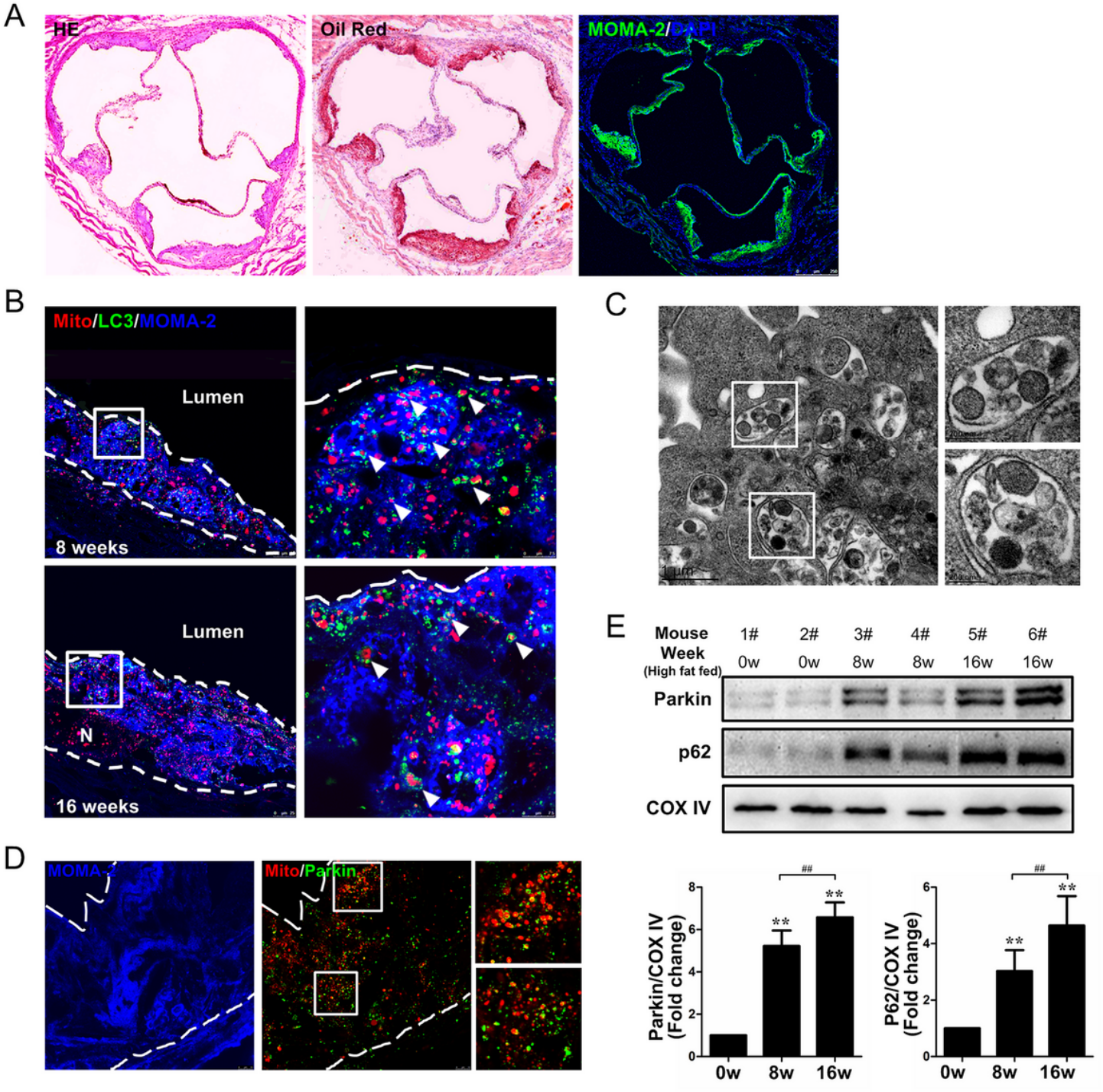

Figure 5

Mitophagy is activated in lesional macrophages of ApoE-/- mice. (A) Adjacent aortic root frozen sections from ApoE-/- mice fed on a western diet for 8 weeks were stained with hematoxylin and eosin (HE), Oil Red (OR) and antibody against MOMA-2 (green fluorescence), respectively. (B) Aortic root sections from ApoE-/- mice fed on a Western diet for 8 or 16 weeks were stained with Mitotracker (red), LC3 antibody (green) and MOMA-2 antibody (blue). The intima of the aortic are outlined with the dotted lines (white). Boxes indicate regions enlarged on the right-hand side, and the arrowheads indicate mitochondria (red) encircled by LC3 puncta (green). N, necrotic core. Scale bar, 25 μm. (C) Representative transmission electron micrographs of the aortic lesions from ApoE-/- mice fed on a western diet for 8 weeks, demonstrating autophagic structures containing partially degraded mitochondria. Boxes indicate regions enlarged on the right. (D) Aortic root sections from ApoE-/- mice fed on a western diet for 8 weeks were immunostained with Mitotracker (red) and Parkin antibody (green); adjacent sections were stained with MOMA-2 antibody (blue) to identify lesional macrophages. Scale bar, 10 μm. (E) Representative immunoblots and densitometric graphs of the mitochondrial content of Parkin and p62 levels (normalized against COX IV) in aorta of ApoE-/- mice fed on a western diet for 0 week (n=4), 8 weeks (n=5) and 16 weeks (n=5). **P<0.01 vs. 0 week; ##P<0.01 between indicated groups. ApoE, apolipoprotein E; LC3, microtubule-associated protein 1 light chain 3; MOMA-2, anti-monocyte + macrophage antibody; COX IV, cytochrome c oxidase subunit IV.

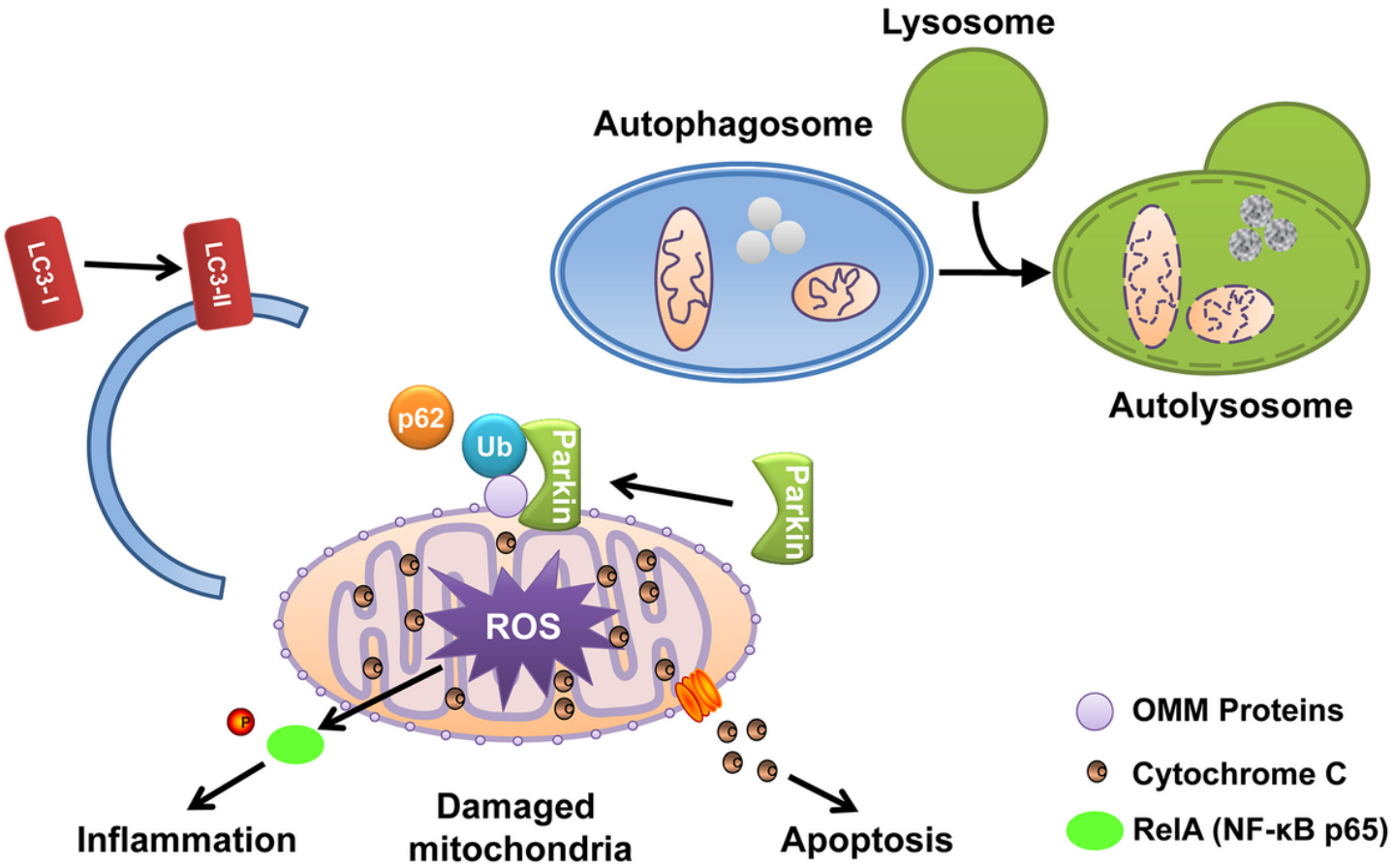

Figure 6

Possible roles of Parkin and mitophagy during atherogenesis.

Supplementary Files

This is a list of supplementary files associated with this preprint. Click to download.

- FigureS1.tiff